ACI STRUCTURAL JOURNAL TECHNICAL PAPER

Title No. 118-S17

High-Strength Steel Bars in Earthquake-Resistant Reinforced Concrete T-Shaped Walls

by Mohammad Sajedul Huq, Erick A. Burgos, Rémy D. Lequesne, and Andrés Lepage

Six large-scale reinforced concrete T-shaped slender walls were tested under reversed cyclic loading to study the effects of reinforcing bar mechanical properties on wall deformation capacity. Effects on lateral stiffness and hysteretic energy dissipation were also quantified. Primary variables included reinforcement yield stress and the ratio of tensile-to-yield strength (f_t/f_y). An additional aim of the tests was to determine the minimum uniform elongation (strain at peak stress) and fracture elongation required of high-strength reinforcing bars for use in earthquake-resistant structures. The walls were not subjected to axial loads other than the weight of the loading apparatus and self-weight.

The T-shaped walls, with a specified concrete compressive strength of 8 ksi (55 MPa), had a 100 in. (2540 mm) long stem joining a single 100 in. (2540 mm) long flange, both 10 in. (254 mm) thick. All walls had a nominal shear span of 300 in. (7620 mm). The control specimen T1 was constructed with conventional Grade 60 (420) reinforcement (where Grade corresponds to the specified yield stress of reinforcement). Walls T2, T3, T4, and T6 were constructed with Grade 100 (690) reinforcement and T5 with Grade 120 (830) reinforcement. Test results showed that regardless of the reinforcement grade, walls designed for similar flexural strength using longitudinal reinforcement with f_t/f_y between 1.18 and 1.39, uniform elongation not less than 6%, and fracture elongation not less than 10% had similar strengths and drift ratio capacities. The effective initial stiffness and hysteretic energy dissipation index for walls with high-strength reinforcement (T2 through T6) were approximately 70%, on average, of those for the wall with conventional reinforcement (T1).

Keywords: deformation capacity; fracture elongation; high-strength reinforcement; reversed cyclic load; slender walls; tensile-to-yield strength ratio; uniform elongation.

INTRODUCTION

ACI 318-14[1] does not permit the use of high-strength reinforcing bars with a nominal yield stress higher than 80 ksi (550 MPa) for purposes other than as transverse reinforcement for confinement. Increased understanding and acceptance of the use of high-strength steel bars could allow designers to reduce the amount of reinforcement in structural members, resulting in more efficient design and less reinforcement congestion.

The main objectives of this study were to determine the effects of the tensile-to-yield strength ratio, uniform elongation, and fracture elongation of high-strength reinforcing bars on the behavior of slender T-shaped reinforced concrete walls for earthquake-resistant construction. This was accomplished by selecting Grade 100 (690) and Grade 120 (830) bars with different stress-strain characteristics for different specimens. The effects of replacing conventional Grade 60 (420) reinforcement with a reduced amount of high-strength Grade 100 (690) or Grade 120 (830) reinforcement were also evaluated using data from tests of large-scale T-shaped concrete walls subjected to reversed cyclic displacements. T-shaped walls were selected because higher tensile strains are expected in the longitudinal reinforcement for this shape than for most others resisting axial and shear forces and bending moment.

RESEARCH SIGNIFICANCE

The available literature on the use of high-strength steel bars as concrete reinforcement in members designed according to U.S. construction practice has focused predominantly on beams[2,3] and columns.[4,5] Previous studies have not investigated the cyclic response of asymmetric concrete walls reinforced with Grade 100 (690) or Grade 120 (830) steel bars available in the United States.

This research provides test data essential for evaluating the use of high-strength reinforcement in slender concrete walls and for studying the effects of reinforcement mechanical properties on wall deformation capacity; mainly the tensile-to-yield strength ratio, uniform elongation (strain at peak stress), and fracture elongation.

EXPERIMENTAL PROGRAM

Results are reported from tests of six large-scale T-shaped walls subjected to uniaxial reversed cyclic displacements patterned after the loading protocol in FEMA 461.[6] Figure 1 shows nominal cross-sectional dimensions and reinforcement details for T1 and Fig. 2 shows the boundary element details for T2 through T6. All walls were 10 in. (254 mm) thick with a 100 in. (2540 mm) long stem intersecting a 100 in. (2540 mm) long flange at one end. Reinforcement ratio in the unconfined flange and stem was not varied. A typical wall elevation and reinforcement layout are shown in Fig. 3 with a nominal overall specimen height of 337 in. (8560 mm). Displacements were applied at a nominal elevation of 300 in. (7620 mm) above the base block, resulting in a shear span-depth ratio of 3.0 (Fig. 4).

The control specimen T1 had Grade 60 (420) reinforcement with a tensile-to-yield strength ratio (f_t/f_y) of 1.34 and 1.39 for the No. 6 and 4 (19 and 13) bars, respectively (refer

ACI Structural Journal, V. 118, No. 1, January 2021.

MS No. S-2020-047, doi: 10.14359/51728091, received February 5, 2020, and reviewed under Institute publication policies.

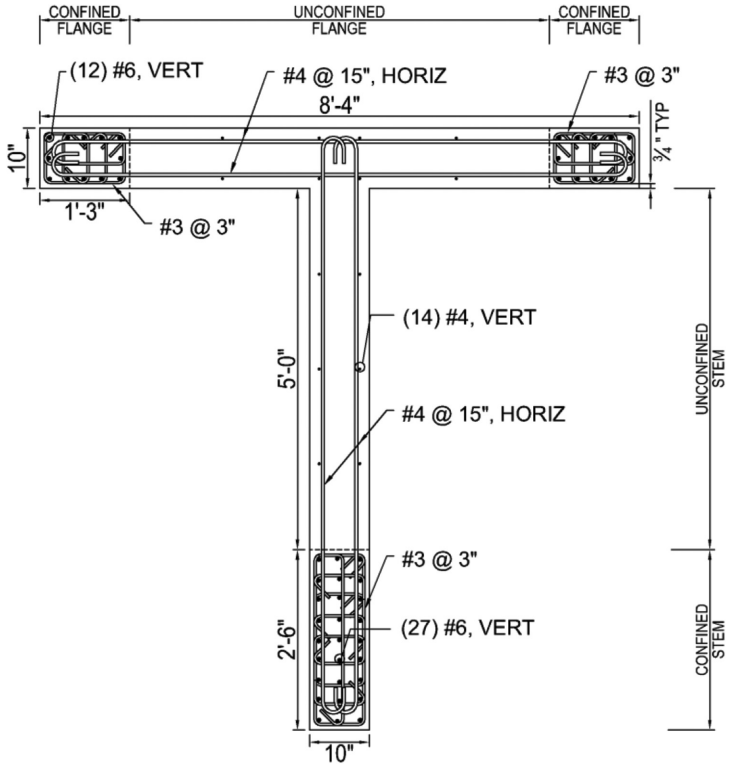

Fig. 1—Wall cross section and reinforcement layout for T1. (Note: 1 in. = 25.4 mm.)

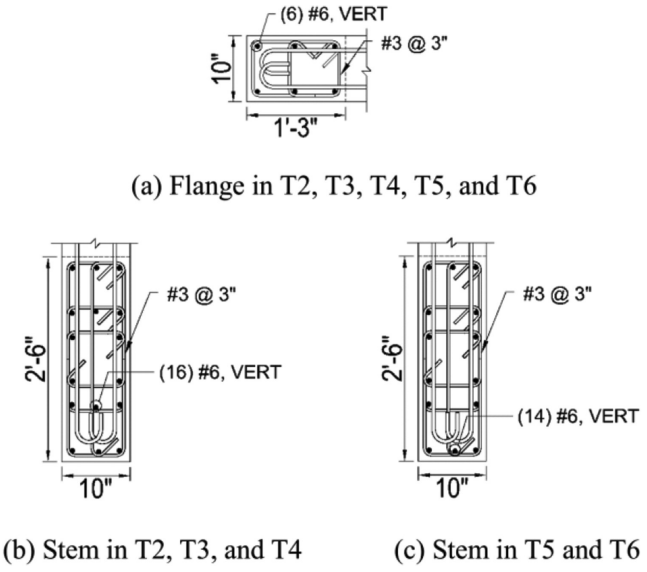

Fig. 2—Confined boundary elements for T2 through T6. (Note: 1 in. = 25.4 mm.)

to Table 1). Walls T2, T3, T4, and T6, which were reinforced with Grade 100 (690) reinforcement, had No. 6 and 4 (19 and 13) bars with f_t/f_y between 1.10 and 1.36. Wall T5 had Grade 120 (830) reinforcement with f_t/f_y of 1.33 and 1.31for the No. 6 and 4 (19 and 13) bars. Uniform and fracture elongations varied as shown in Table 1. More detailed information regarding the experimental program are provided in Huq et al.[9] and Burgos et al.[10]

Specimen design

The walls were designed so their strength would be limited by flexural yielding. The specimens had similar nominal flexural strengths based on specified material properties. The longitudinal reinforcement ratio (ρ_ℓ) for T2 through T4 was decreased in the boundary elements in inverse proportion to the specified reinforcement yield stress to achieve nearly the same $\rho_\ell f_y$ of the control specimen T1. For T5, with Grade 120 (830) reinforcement, ρ_ℓ in the stem boundary element was also reduced to maintain nearly the same $\rho_\ell f_y$. Wall T6 had the same reinforcement layout as T5, except that T6 used Grade 100 (690) bars. The nominal compressive strength (f_c') of concrete for all walls was 8 ksi.

The control specimen T1 had a design flexural strength that resulted in a shear force demand similar to the design shear strength associated with the minimum transverse reinforcement ratio (ρ_t) required by ACI 318-14[1] for special structural walls ($\rho_{t,min}$ = 0.25%). The wall was therefore designed to have $0.9M_n$ approximately equal to $0.6V_nh_w$, where M_n and V_n correspond to calculated nominal strengths for flexure and shear, based on h_w = 300 in. (7620 mm) and specified material properties. The 0.9 and 0.6 factors are the strength reduction factors in ACI 318-14[1] for flexure and shear in tension-controlled special structural walls. The shear stress demand associated with the probable flexural strength of the walls (calculated using 1.25 times the specified yield stress of the reinforcement) did not exceed $4\sqrt{f_c'}$, psi ($0.33\sqrt{f_c'}$, MPa). All walls (T1 through T6) had the same ρ_t, consisting of No. 4 (13) bars spaced at 15 in. (380 mm) in two layers.

The walls were designed to satisfy the detailing requirements in ACI 318-14[1] for special structural walls. In addition, the walls with Grade 100 (690) or Grade 120 (830) reinforcement followed recommendations in ATC 115[11] that limit the spacing of the confining reinforcement in boundary elements to 4 times the diameter of the longitudinal bars.

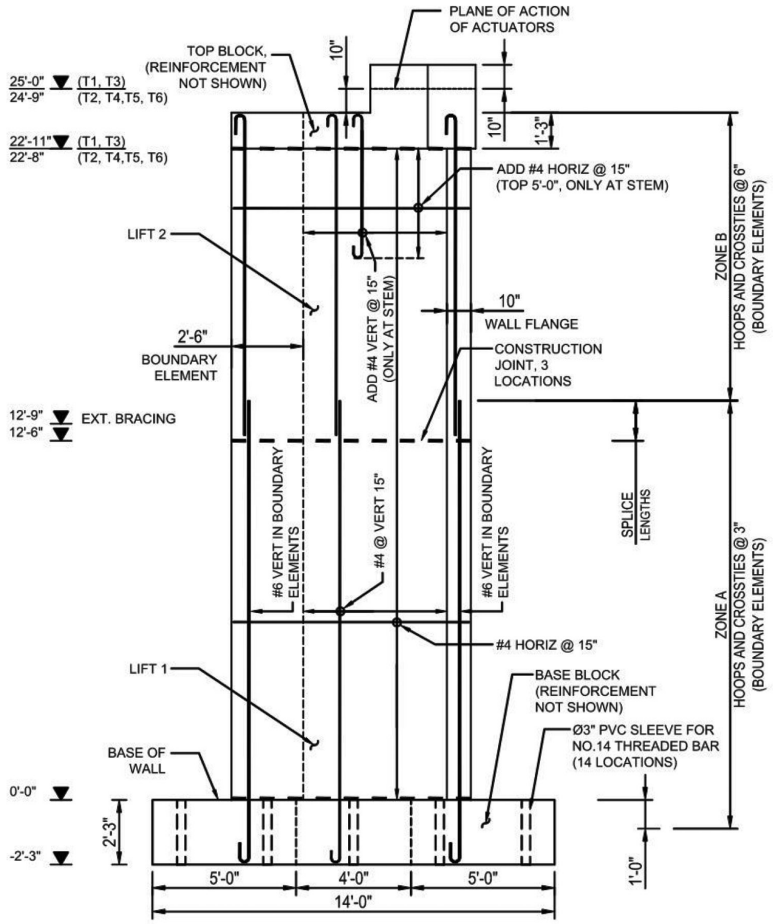

Fig. 3—Typical wall elevation and reinforcement layout. (Note: 1 in. = 25.4 mm.)

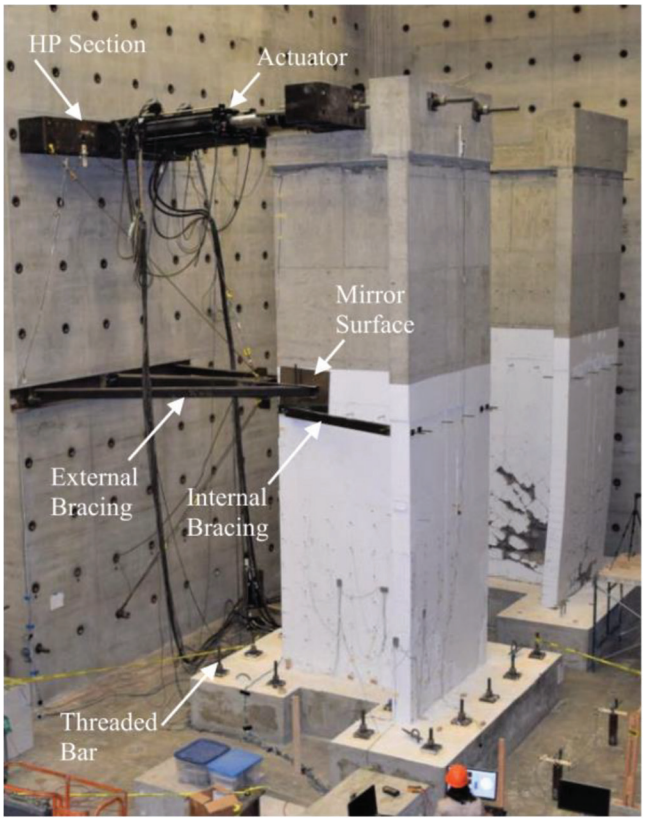

Fig. 4—Test setup.

Specimen construction

Each specimen was constructed in four stages (base block, Lift 1, Lift 2, and top block) with three construction joints (Fig. 3). Each stage consisted of assembling reinforcing bar cages and wooden formwork, followed by concrete placement and curing. Formwork was typically removed three to four days after casting. The concrete surface at construction joints was intentionally roughened to enhance the shear transfer mechanism. Concrete cylinders were made to monitor the concrete strength for each placement. The cylinders were kept inside the laboratory in the same environmental conditions as the specimens until test day.

The grade of reinforcement used in Lifts 1 and 2 were the same. The base and top blocks were built with nominally identical detailing using Grade 60 (420) reinforcement in all specimens. Wall longitudinal reinforcement was lap spliced near midheight above the construction joint between Lift 1 and Lift 2, as shown in Fig. 3. The splice lengths were determined based on Eq. (4-11a) of ACI 408R-03[12] with $\phi = 0.82$ and nominal f_y.

Material properties

All reinforcement consisted of deformed steel bars. According to the mill test reports, reinforcement in T1 was compliant with ASTM A706[13] Grade 60 (420), while that of T2, T3, T4, and T6 was compliant with ASTM A615[14] Grade 100 (690), and reinforcement in T5 was compliant

Table 1—Reinforcing steel properties

Wall	Bar designation No.	Nominal bar diameter in. (mm)	Yield stress f_y,* ksi (MPa)	Tensile strength f_t,† ksi (MPa)	f_t/f_y	Uniform elongation ε_{su}‡	Fracture elongation ε_{sf}†
T1	6 (19)	0.75 (19)	70 (483)	94 (648)	1.34	12.1%	15.0%§
	4 (13)	0.50 (13)	76 (524)	106 (731)	1.39	10.6%	14.0%§
	3 (10)	0.375 (10)	60 (414)§	91 (627)§	1.52	—	16.5%§
T2	6 (19)	0.75 (19)	108 (745)	124 (855)	1.15	8.9%	13.0%§
	4 (13)	0.50 (13)	108 (745)	119 (820)	1.10	5.5%	10.0%§
	3 (10)	0.375 (10)	109 (752)§	134 (924)§	1.23	—	11.3%§
T3	6 (19)	0.75 (19)	99 (683)	122 (841)	1.23	9.1%	12.5%§
	4 (13)	0.50 (13)	101 (696)	122 (841)	1.21	5.8%	12.5%§
	3 (10)	0.375 (10)	109 (752)§	134 (924)§	1.23	—	11.3%§
T4	6 (19)	0.75 (19)	96 (662)	131 (903)	1.36	8.5%	12.5%§
	4 (13)	0.50 (13)	107 (738)	128 (883)	1.20	6.2%	10.9%§
	3 (10)	0.375 (10)	109 (752)§	134 (924)§	1.23	—	11.3%§
T5	6 (19)	0.75 (19)	129 (889)	171 (1179)	1.33	5.4%	9.9%
	4 (13)	0.50 (13)	127 (876)	167 (1151)	1.31	5.3%	8.6%
	3 (10)	0.375 (10)	140 (965)	174 (1200)	1.24	—	7.3%
T6	6 (19)	0.75 (19)	112 (772)	132 (910)	1.18	7.1%	10.1%
	4 (13)	0.50 (13)	109 (752)	134 (924)	1.23	7.3%	9.7%
	3 (10)	0.375 (10)	140 (965)	174 (1200)	1.24	—	7.3%

*Yield stress based on 0.2% offset method following ASTM A370,[7] unless otherwise noted.

†Following ASTM A370[7] and using an 8 in. (203 mm) gauge length, unless otherwise noted.

‡Strain at maximum tensile stress, following ASTM E8[8] and using an 8 in. (203 mm) gauge length.

§Based on mill test report.

with ASTM A1035[15] Grade 120 (830). Figure 5 shows tensile test results for No. 6 (19) bars used as longitudinal reinforcement in the confined boundary elements and No. 4 (13) bars used in the unconfined regions of the walls. Table 1 lists the measured yield and tensile strengths of the reinforcement used in the walls (excluding the bottom and top blocks). Also listed are the uniform and fracture elongations determined according to ASTM E8[8] and ASTM A370,[7] respectively.

Concrete with a target compressive strength of 8 ksi (55 MPa) was provided by a local ready mix plant. Table 2 lists the measured concrete compressive strengths for the various concrete placements. Standard cylinders were tested following ASTM C39[16] and ASTM C496[17] within a few days of the actual specimen test day.

Test setup

The specimens were anchored to the laboratory strong floor using 14 No. 14 (43) Grade 100 (690) threaded bars passing through the 27 in. (686 mm) deep base block. The top of each specimen was connected to two hydraulic actuators (Fig. 4) acting in parallel at the same elevation. Each actuator had a stroke length of 40 in. (1020 mm) and a force capacity of 220 kip (980 kN) in tension and 330 kip (1460 kN) in compression. The actuators were spaced 54 in. (1372 mm) apart and centered with respect to the wall stem, which provided resistance to possible twisting of the specimens during testing. The actuators were attached on one end to the strong wall and on the other to the top block by means of HP18 steel sections. Steel fixtures that braced the wall near midheight, shown in Fig. 4, included: 1) internal bracing to prevent local section distortion (relative movement between stem and flange); and 2) external bracing to prevent global twisting. Friction between the external bracing and the specimen was minimized by using a nylon pad bearing on a mirror-finished steel plate attached to each side of the wall stem. The walls were not subjected to axial loads other than the tributary weight of the loading apparatus (6.8 kip [30.3 kN]) and the self-weight of the specimen above the base block (54.1 kip [241 kN]), for a total load of approximately 61 kip (271 kN) at the base of the wall. Before setting up the instrumentation, the specimens were painted with an oil-based white paint to facilitate the marking of cracks during testing.

Instrumentation

Lateral deflection at the top of the specimens, relative to the laboratory strong wall, was measured with three string potentiometers installed 10 in. (254 mm) below the plane of action of the actuators. Two of the potentiometers, with a 40 in. (1020 mm) stroke, were spaced 72 in. (1830 mm) apart to measure lateral displacement and twisting of the specimen. The third potentiometer, with a 20 in. (508 mm) stroke, was installed at the centerline of the wall as a redundant measurement. Two potentiometers with a 4 in. (102 mm) stroke were attached to the base block at 19 in. (483 mm) above the

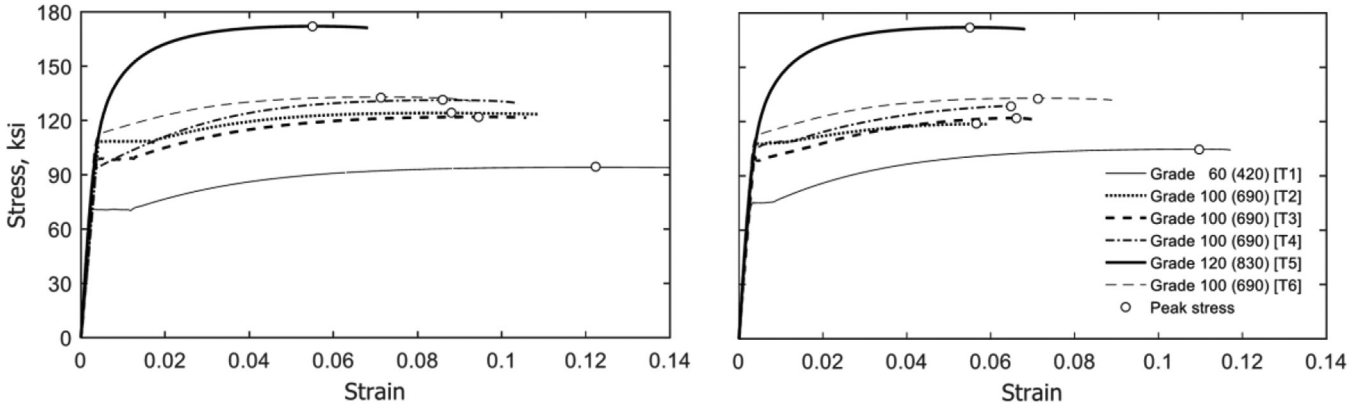

Fig. 5—Measured stress versus strain for longitudinal bars. (Note: 1 ksi = 6.89 MPa.)

Table 2—Measured concrete strengths at test day

Wall	Measured strength,* ksi (MPa)	Bottom block	Wall Lift 1	Wall Lift 2	Lift average	Top block
T1	f_{cm}†	8.0 (55)§	7.2 (50)	7.4 (51)	7.3 (50)	6.8 (47)
	f_{ct}‡	–	0.55 (3.8)	0.46 (3.2)	0.51 (3.5)	0.50 (3.4)
T2	f_{cm}†	6.9 (48)§	7.9 (54)§	7.7 (53)§	7.8 (54)	6.4 (44)§
	f_{ct}‡	0.42 (2.9)§	0.48 (3.3)§	0.48 (3.3)§	0.48 (3.3)	0.46 (3.2)§
T3	f_{cm}†	7.6 (52)§	7.3 (50)	7.2 (50)§	7.3 (50)	5.4 (37)§
	f_{ct}‡	–	0.52 (3.6)	0.54 (3.7)	0.53 (3.7)	0.39 (2.7)
T4	f_{cm}†	7.4 (51)§	8.6 (59)§	7.2 (50)§	7.9 (54)	6.6 (46)§
	f_{ct}‡	0.52 (3.6)	0.52 (3.6)	0.54 (3.7)	0.53 (3.7)	0.44 (3.0)
T5	f_{cm}†	6.6 (46)§	7.5 (52)	7.6 (52)	7.5 (52)	7.8 (54)
	f_{ct}‡	0.61 (4.2)	0.61 (4.2)	0.62 (4.3)	0.61 (4.2)	0.61 (4.2)
T6	f_{cm}†	7.3 (50)	7.3 (50)	9.2 (63)	8.2 (57)	7.5 (52)
	f_{ct}‡	0.51 (3.5)	0.66 (4.6)	0.70 (4.8)	0.68 (4.7)	0.59 (4.1)

*Batched proportions of concrete mixtures are reported elsewhere.[9,10]

†Compressive strength of concrete following ASTM C39,[16] based on the average of two 6 x 12 in. (150 x 300 mm) cylinders, unless otherwise noted.

‡Splitting tensile strength of concrete following ASTM C496,[17] based on the average of two 6 x 12 in. (150 x 300 mm) cylinders, unless otherwise noted.

§Reported value based on average of three 4 x 8 in. (100 x 200 mm) cylinders.

laboratory strong floor and spaced 72 in. (1830 mm) apart to measure horizontal sliding and twisting of the base block relative to the floor.

For each specimen, additional instrumentation included up to 34 electrical resistance strain gauges on longitudinal and transverse reinforcing bars; four vertical potentiometers, two in series along each of the outer edges of the walls (for calculation of wall elongation and flexural rotation); and two potentiometers in an X pattern on the wall stem (for calculation of the shear distortion in the top two-thirds of the wall). Furthermore, an infrared-based non-contact position measurement system recorded the positions in three-dimensional space of optical markers fixed to the specimen web and flange in a square grid, nominally spaced at 14 in. (356 mm), throughout the bottom one-third of the walls. More details on the instrumentation layout and analysis of test data to quantify the distribution of deformations along the shear span of the walls are reported elsewhere.[9,10]

Loading protocol

A series of fully reversed cyclic displacements were imposed following the protocol shown in Fig. 6, which was patterned after the loading protocol in FEMA 461.[6] The displacement history corresponds to a target drift ratio varying from 0.2 to 4%. The target drift ratio was taken as the top lateral displacement with respect to the base block divided by the distance from the top of the base block to the point of displacement measurement. For each loading step, two displacement cycles were applied. The first half cycle of each step (positive drift ratio) induced compression in the stem. The two actuators acted under displacement control throughout the tests and always imposed equal displacements to prevent global twisting.

During the tests, target drift ratios were based on displacements measured at the top of the wall neglecting base block rotation (due to overturning moment). The actual drift ratios

(described below) were therefore generally lower than the target drift ratios.

TEST RESULTS

Measured shear versus drift ratio

Drift ratio (*DR*) was defined as the relative displacement between the top block (δ_{top}) and base block (δ_{base}) divided by the height of the wall (h_y) and corrected for rotation of the base block (θ_{base})

$$DR = \frac{\delta_{top} - \delta_{base}}{h_y} - \theta_{base} \quad (1)$$

The value of h_y is the distance from the top of the base block to the level where δ_{top} was measured, nominally 10 in. (254 mm) below the plane of action of the actuators. The measured shear force versus drift ratio data are shown in Fig. 7 for T1 through T6. The figures identify the shear force (V_e) associated with the calculated nominal flexural strength (M_n) based on measured material properties (f_{cm} and f_y). The value of M_n was calculated in accordance with Chapter 22 of ACI 318-14,[1] where the maximum stress in reinforcing steel is limited to its yield stress and the maximum strain in the compressed concrete is limited to 0.003. With the exception of T2, which had longitudinal bars with f_t/f_y as low as 1.10 (Table 1), all walls reached a lateral strength higher than V_e.

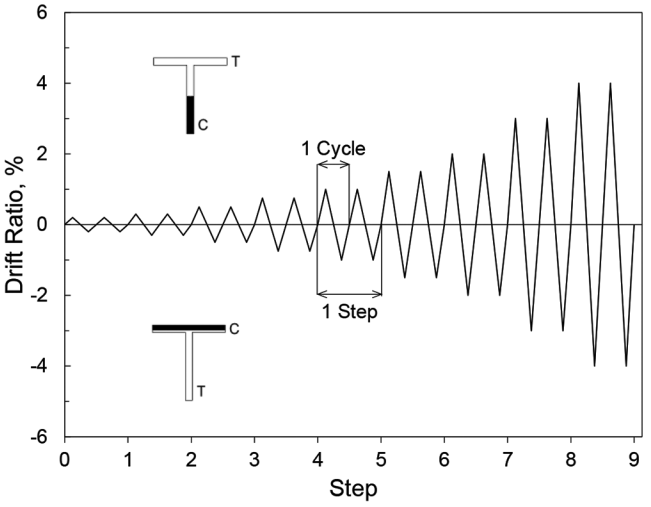

Fig. 6—Loading protocol.

The data in Fig. 7 show that only walls T2 and T5 were not capable of sustaining 80% of their lateral strength for at least one cycle to 3% drift ratio. It is important to note that longitudinal bars in T2 and T5 had uniform elongation (ε_{su}) below 6% (Table 1). The deformation capacities of T2 and T5 were limited by fracture of longitudinal bars without any indication of bar buckling in previous loading cycles. This was not the case for the other walls (T1, T3, T4, and T6), which exhibited bar buckling followed by bar fracture and strength loss.

The maximum measured forces and *DR* for each wall is given in Table 3. Although the walls were designed to have nearly the same flexural strength (with similar $\rho_\ell f_y$), V_{max} in Table 3 varied between 275 and 303 kip (1220 and 1350 kN) for positive drift ratios (excluding T5, which had higher $\rho_\ell f_y$ in the flange). Differences in lateral strength were in part attributable to the combined effects of the tensile-to-yield strength ratio and deviations between the specified and actual yield stress of the longitudinal reinforcement.

According to ASCE 41,[18] well-detailed flexurally controlled reinforced concrete walls subjected to low axial stress ($\leq 0.1 f_{cm}$) and shear stress ($\leq 4\sqrt{f_{cm}}$ psi [$0.33\sqrt{f_{cm}}$ MPa]),

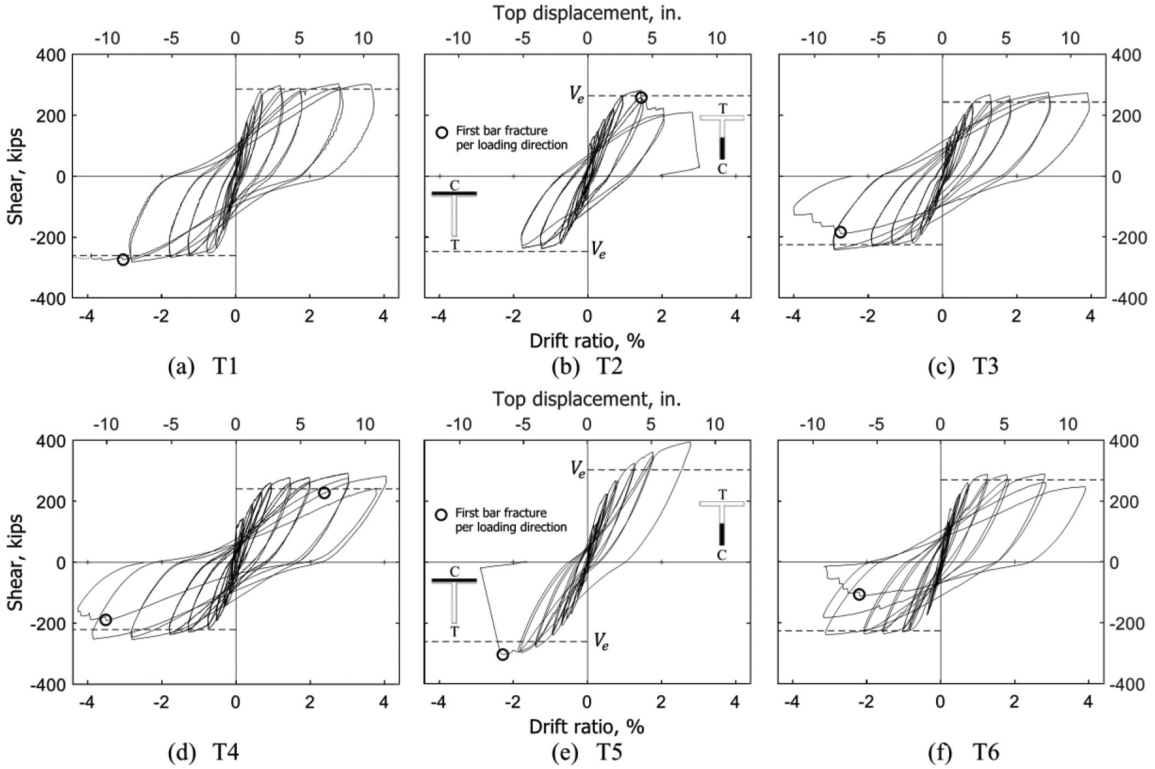

Fig. 7—Shear versus drift ratio. (Note: 1 in. = 25.4 mm; 1 kip = 4.45 kN.)

Table 3—Specimen shear strengths and drift ratio capacities

Wall	V_{max}*, kip (kN)		v_{max}†, $\sqrt{f_{cm}}$ psi (MPa)		DR_{max}‡, %		DR_{cap}§, %
	–	+	–	+	–	+	
T1	282 (1250)	303 (1350)	3.3 (0.27)	3.5 (0.29)	6.00‖	3.73	3.7
T2	237 (1050)	282 (1250)	2.7 (0.22)	3.2 (0.27)	1.80	2.05	1.8
T3	242 (1080)	275 (1220)	2.8 (0.24)	3.2 (0.27)	2.95	3.95	3.0
T4	253 (1130)	293 (1300)	2.8 (0.24)	3.3 (0.27)	3.87	4.05	3.9
T5	303 (1350)	395 (1760)	3.5 (0.28)	4.6 (0.38)	2.30	2.80	2.3
T6	240 (1070)	290 (1290)	2.7 (0.22)	3.2 (0.27)	3.10	3.90	3.1

*Maximum measured shear force per loading direction.

†Shear stress = $V_{max} / (\ell_w t_w \sqrt{f_{cm}})$, where t_w = 10 in. (254 mm); ℓ_w = 100 in. (2540 mm); and f_{cm} is based on lift average in Table 2.

‡Maximum drift ratio attained in loading direction while maintaining shear force not less than $0.8V_{max}$.

§Drift ratio capacity defined as the minimum DR_{max}.

‖After bar fracture in confined stem at approximately –3.1% drift ratio (during first cycle to a target drift ratio of 4%), unidirectional loading continued until reaching capacity of testing apparatus.

should exhibit a plastic hinge rotation of 1.5% before significant strength degradation occurs. Based on values of DR_{cap} in Table 3 and given that the walls with high-strength reinforcement yielded at drift ratios near 1%, T1, T3, T4, and T6 exhibited plastic hinge rotations that exceeded the 1.5% value recommended in ASCE 41.[18] Recommended minimum values for ε_{su}, ε_{sf}, and f_t/f_y should therefore be based on the mechanical properties of the reinforcement used in T1, T3, T4, and T6.

Progression of damage

The first cracks were due to flexure and occurred at a drift ratio of approximately 0.2%. New cracks developed through drift ratios of 3%, after which the existing cracks continued to widen. Additional details and photos are provided elsewhere.[9,10]

Table 4 identifies the drift cycle and wall region where bar buckling and bar fracture were first observed in each wall. For all walls, concrete flaking and minor spalling at the tip of the stem was first observed during the first cycle to 1% drift ratio. For T2 and T5, bar fracture of longitudinal bars (typically leading to a significant loss in lateral resistance) occurred before bar buckling. The other walls (T1, T3, T4, and T6) exhibited fracture of longitudinal bars in the confined stem that was preceded by buckling of the same bars during prior cycles. Buckling of the longitudinal reinforcement in the confined stem was first observed as indicated in Table 4: for T1 and T6, during the second cycle to a drift ratio of 3%; for T3, during the first cycle to a drift ratio of 4%; and for T4, during the second cycle to a drift ratio of 4%. All of the events documented in Table 4 occurred near the base of the walls.

Table 4 shows that bar fracture often occurred during the first or second cycle of loading after bar buckling was first noted—especially within the confined boundary elements. However, not all bars that buckled in the unconfined regions fractured in subsequent cycles. This may be because the longer buckling length (of bars in unconfined regions) reduced the bar curvature demand associated with buckling.

The relatively lower deformation capacity of T2 and T5 was mostly due to their failure mechanisms, which were different from the other walls. In T2, none of the Grade 100 (690) longitudinal bars that fractured had buckled in prior cycles; instead, there was a concentration of tensile strain demands at one of the flexural cracks near the base of the unconfined flange. As crack opening progressed, the No. 4 (13) bars in the flange-stem intersection fractured. This was followed by fracture of additional No. 4 (13) bars in the unconfined stem and then fracture of all No. 6 (19) bars in one of the confined flanges. In contrast, T5 failed due to fracture of the No. 6 (19) Grade 120 (830) longitudinal bars in the confined stem, also without exhibiting prior buckling. It is very likely that additional confining reinforcement would not have improved the deformation capacity of T2 or T5 given the mode of failure.

Effect of steel mechanical properties on drift ratio capacity

To identify the minimum tensile-to-yield strength ratio, uniform elongation, and fracture elongation required of high-strength reinforcement for acceptable performance, Fig. 8 shows drift ratio capacity versus uniform elongation (ε_{su}) and fracture elongation (ε_{sf}). Walls were deemed to have acceptable performance if they behaved equal or better than T1. Specifically, having a deformation capacity not less than 3%, the drift ratio at which T1 first exhibited bar fracture (Fig. 7(a)), and a failure mode that included bar fracture only after buckling was observed.

The data in Fig. 8 also include values of f_t/f_y that correspond to the longitudinal bars that fractured and limited the wall deformation capacity. These bars were No. 6 (19) for T1, T3, T4, T5, and T6 in the confined stem, and No. 4 (13) for T2 in the unconfined flange. Figure 8 shows that drift ratio capacity was somewhat correlated with ε_{su} and ε_{sf}. Furthermore, within pairs of specimens with similar ε_{su}, such as T2-T5 and T3-T4, the specimens with greater f_t/f_y exhibited greater drift ratio capacity. Based on these limited data, ε_{su}, ε_{sf}, and f_t/f_y all appear to be relevant to wall deformation capacity. The data in Fig. 8 suggest that sudden bar fracture is not likely and drift ratio capacity is likely to exceed 3% for slender well-detailed walls with low axial and shear stresses

Table 4—Drift cycle and location of longitudinal bar where bar buckling or bar fracture was first observed

Wall	Bar location*		Drift cycle†											
			2%				3%				4%			
			i+	i–	ii+	ii–	i+	i–	ii+	ii–	i+	i–	ii+	ii–
T1	Flange	Unconfined		B										
		Confined												
	Stem	Unconfined										B		
		Confined							B			F		
T2	Flange	Unconfined	F											
		Confined					F							
	Stem	Unconfined	F											
		Confined												
T3	Flange	Unconfined										B		
		Confined												
	Stem	Unconfined				B								
		Confined									B	F		
T4	Flange	Unconfined‡								B	F			
		Confined												
	Stem	Unconfined‡												
		Confined											B	F
T5	Flange	Unconfined												
		Confined												
	Stem	Unconfined						F						
		Confined						F						
T6	Flange	Unconfined								B				
		Confined												
	Stem	Unconfined										F		
		Confined							B	F				

*Confined region refers to boundary element with closely spaced transverse reinforcement. Unconfined flange includes the intersection of flange and stem (refer to Fig. 1).

†Notation: i+ is first cycle, stem in compression; i– is first cycle, stem in tension; ii+ is second cycle, stem in compression; ii– is second cycle, stem in tension; B is buckling of longitudinal reinforcement; F is fracture of longitudinal reinforcement. Reported events (B and F) all occurred near the base of the wall.

‡Concrete cover to No. 4 (13) longitudinal bars in unconfined regions was 2.38 in. (60 mm) for T4 and 1.38 in. (35 mm) for other walls. Concrete cover to No. 4 (13) transverse bars in unconfined regions was 1.88 in. (48 mm) for all walls.

and longitudinal reinforcement having $f_t/f_y \geq 1.18$, $\varepsilon_{su} \geq 6\%$, and $\varepsilon_{sf} \geq 10\%$.

Stiffness

Two stiffness measures were determined for each wall, the effective initial stiffness (K_e) and the unloading stiffness (K_u). Wall stiffness was defined as the lateral force required at the top of the wall to reach a unit displacement with respect to the base of the wall. The level of displacement measurement was located 10 in. (254 mm) below the level at which the load was applied. For each of the six walls, stiffness measurements were determined using data from the measured shear versus drift ratio, after converting drift ratios to displacements (Fig. 7).

For reinforced concrete members, stiffness K_e represents the secant stiffness to the notional yield point (Δ_y, F_y) generally used in the definition of an idealized force-displacement curve (Fig. 9) with a bilinear backbone and a stiffness-reducing hysteresis model. The idealized hysteresis in Fig. 9 is representative of reinforced concrete members subjected to cyclic loading, where the unloading and reloading stiffness decrease with increased maximum displacement.[19]

The notional yield point to define $K_{e,meas}$ for the wall specimens was taken at a shear equal to $0.8V_{max}$ for each loading direction. The coefficient of 0.8 consistently identified the onset of a significant reduction in stiffness,[9,10] as indicated by the initial segments of the shear versus drift ratio envelopes in Fig. 10.

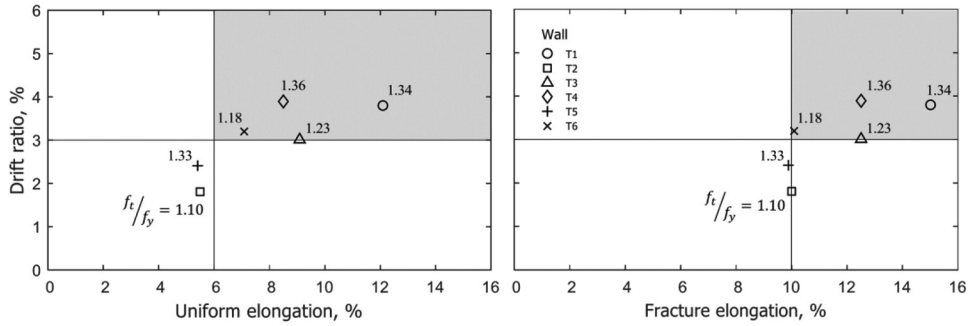

(a) Drift ratio vs. uniform elongation (b) Drift ratio vs. fracture elongation

Fig. 8—Drift ratio capacity versus elongation of longitudinal bar controlling wall drift capacity.

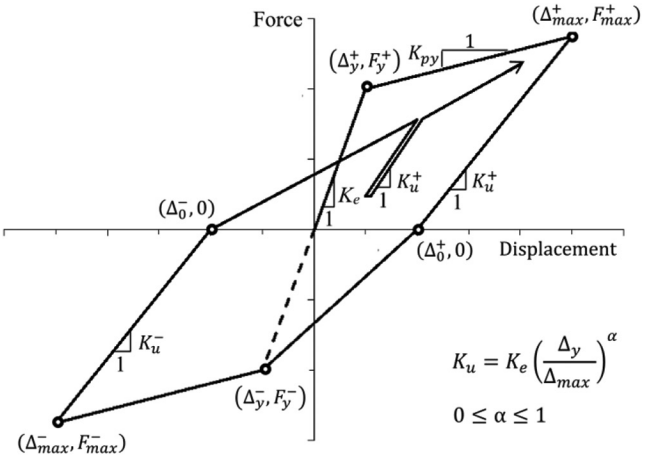

Fig. 9—Idealized force-displacement curve and hysteresis model.

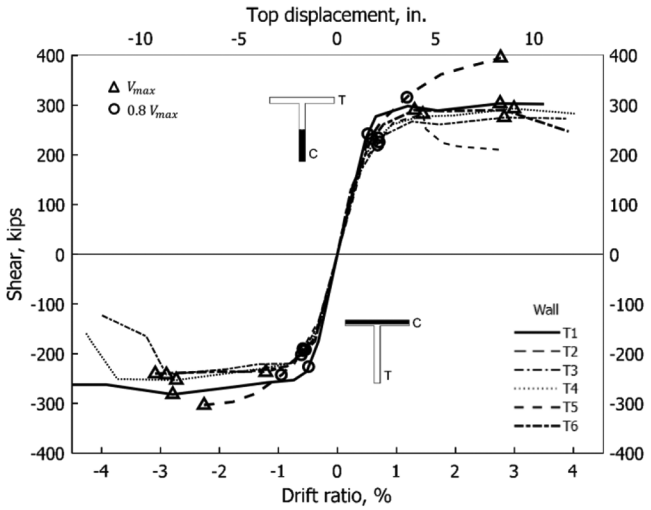

Fig. 10—Shear versus drift ratio envelopes. (Note: 1 in. = 25.4 mm; 1 kip = 4.45 kN.)

A procedure to calculate the effective initial stiffness $K_{e,calc}$ for each wall is documented in Table 5, where all of the relevant parameters are listed. The table includes $K_{e,meas}$ obtained from Fig. 10, after converting drift ratios to displacements. $K_{e,calc}$ accounts for deformations due to flexure, shear, and strain penetration, assuming cracked section properties throughout the height of the wall. The ratios of measured-to-calculated stiffness at the bottom

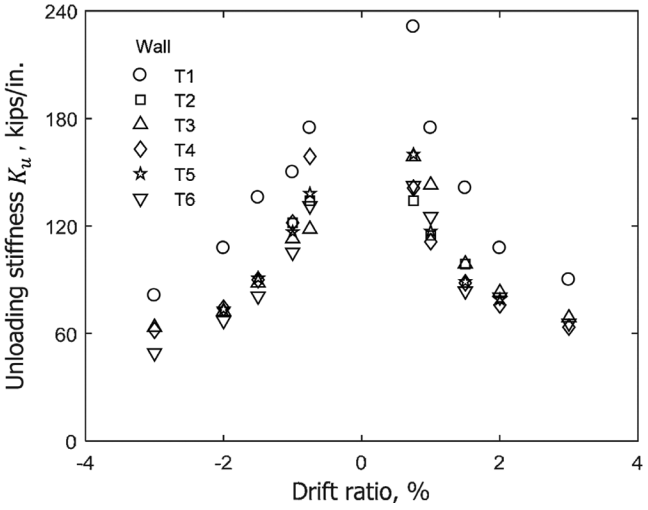

Fig. 11—Unloading stiffness versus drift ratio. (Note: 1 in. = 25.4 mm; 1 kip = 4.45 kN.)

of Table 5 ranged between 0.82 and 1.13, with a mean of 0.96, indicating that the procedure to determine $K_{e,calc}$ gave similar (but slightly higher, on average) values than $K_{e,meas}$, an outcome consistent with observations by others.[21,22] Note that on average, the value of K_e (both measured and calculated) for walls with high-strength reinforcement (T2 through T6) was nearly 70% of the values of K_e for the wall with conventional reinforcement (T1). The stiffness of the walls was nearly proportional to the longitudinal reinforcement ratio, which, for most specimens, was inversely proportional to the specified yield stress.

The calculated flexural stiffness based on uncracked gross section properties was 1070 kip/in. (187 kN/mm) for T1 and an average of 1100 kip/in. (193 kN/mm) for walls with high-strength reinforcement (T2 through T6). These stiffness values were calculated using the same moment of inertia but different values of h_w, h_y, and f_{cm} (reported in Table 5). Given that the average of $K_{e,meas}$ was 163 kip/in. (28.5 kN/mm) for T1 and 114 kip/in. (20.0 kN/mm) for T2 through T6, the average ratio of measured-to-calculated stiffness based on gross moment of inertia was 15% for T1 and 10% for T2 through T6. These ratios are consistent with values reported in ATC 72[23] for reinforced concrete members with axial load at or below $0.1f_c'A_g$.

The unloading stiffness (K_u) was defined as the secant stiffness from the maximum drift during a half cycle of

Table 5—Wall data for cracked stiffness calculation

Term*	Direction	Unit	Wall					
			T1	T2	T3	T4	T5	T6
h_w		in.	300	297	300	297	297	297
h_y		in.	290	287	290	287	286	286
ℓ_w		in.	100	100	100	100	100	100
t_w		in.	10	10	10	10	10	10
f_y†		ksi	70	108	99	96	129	112
E_s		ksi	29,000	29,000	29,000	29,000	29,000	29,000
f_{cm}‡		ksi	7.3	7.8	7.3	7.9	7.5	8.2
E_c§		ksi	4870	5030	4870	5070	4940	5160
G_c‖		ksi	2030	2100	2030	2110	2060	2150
$X_{cg,cr}$	+	in.	28.9	23.7	23.9	23.6	23.9	23.5
	–	in.	10.2	8.1	8.2	8.0	7.7	7.5
I_{cr}	+	in.^{4}	421,000	262,000	269,000	260,000	266,000	256,000
	–	in.^{4}	446,000	270,000	278,000	268,000	244,000	234,000
ϕ_K			1/10	1/10	1/10	1/10	1/10	1/10
λ#			8	15	13	13	20	16
K_f**	+	kip/in.	240	159	153	159	159	160
	–	kip/in.	254	164	158	164	146	146
K_v††		kip/in.	700	732	700	735	720	752
K_{sp}‡‡	+	kip/in.	3930	1370	1540	1590	1030	1300
	–	kip/in.	4160	1420	1600	1630	950	1180
$K_{e,calc}$§§	+	kip/in.	171	119	116	121	116	120
	–	kip/in.	178	122	119	124	108	111
$K_{e,meas}$‖‖	+	kip/in.	163	113	113	119	96	136
	–	kip/in.	162	114	115	117	89	124
$K_{e,meas}/K_{e,calc}$	+		0.95	0.95	0.97	0.98	0.83	1.13
	–		0.91	0.93	0.97	0.94	0.82	1.12

*For notation and definitions, refer to Notation section.

†Measured yield stress of the main flexural reinforcement, No. 6 (19) bar from Table 1.

‡Measured average compressive strength of concrete, lift average in Table 2.

§Modulus of elasticity of concrete, $57\sqrt{1000 f_{cm}}$ ksi.

‖Shear modulus of concrete, $E_c/2.4$.

#From $2\lambda = \ell_d / d_b$ where ℓ_d is based on Eq. (4-11a) in ACI 408R-03[12] using $\phi = 1$, $\omega = 1$, $\alpha = \beta = \lambda = 1$ and $(c\omega + K_{tr})/d_b = 4$: $\ell_d / d_b = (1000 f_y / f_c'^{1/4} - 2400)/305$, where $f_c' = 1000 f_{cm}$ of the base block in Table 2.

**From flexural deflection Δ_f at elevation h_y of a cantilever beam with flexural rigidity $E_c I_{cr}$ and subjected to point load V at h_w: $\Delta_f = V h_y^2 (3h_w - h_y)/(6E_c I_{cr})$.

††From shear deflection at elevation h_y of a cantilever beam with shear rigidity $G_c \ell_w t_w \phi_K$ and subjected to point load V at h_w. The term ϕ_K was taken as 1/10; refer to 7.14 (Shear Stiffness) in Moehle[20]: $\Delta_v = V h_y / (G_c \ell_w t_w \phi_K)$.

‡‡From deflection due to strain penetration Δ_{sp} at elevation h_y assuming an additional curvature of $V h_w / (E_c I_{cr})$ over a distance λd_b lumped at the base of the wall: $\Delta_{sp} = V h_w h_y \lambda d_b / (E_c I_{cr})$.

§§Calculated stiffness of wall, $K_{e,calc} = 1/(1/K_f + 1/K_v + 1/K_{sp})$.

‖‖Measured stiffness based on secant to $0.8V_{max}$, from shear-drift envelope[9,10] (Fig. 10).

Note: 1 in. = 25.4 mm; 1 kip = 4.45 kN.

loading to the drift reached when unloaded to zero shear, as represented in Fig. 9. The data in Figure 11 shows K_u versus target drift ratio (between 0.75% and 3%), where K_u was determined using the peak drift and the associated shear measured during second cycles of the loading steps (Fig. 6). Regardless of the reinforcement grade, K_u was reduced by a factor of approximately 0.6 when the drift ratio increased from 1% to 3%. On average, for the same target drift ratio in both loading directions, the value of K_u for walls with high-strength reinforcement (T2 through T6) was approximately 70% of the value of K_u for the wall with conventional reinforcement (T1).

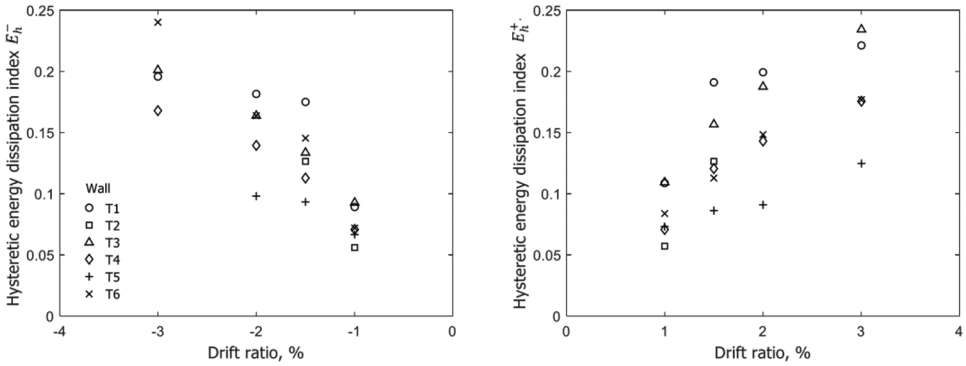

Fig. 12—Hysteretic energy dissipation index versus drift ratio.

Hysteresis

Test data were also used to calculate the hysteretic energy dissipation index[19]

$$E_h = \left(\frac{W}{\pi \Delta_m V_m} \right) \quad (2)$$

The index E_h represents the equivalent viscous damping factor of a linear-elastic system capable of dissipating energy W under steady-state oscillation.[19] The amount of hysteretic energy W is calculated per half cycle for each loading direction resisting a force V_m at the peak displacement Δ_m. The value of W was calculated as the area enclosed by the measured shear versus drift curve and $V = 0$ for a given half cycle. Figure 12 shows the values of E_h for the positive and negative loading directions associated with the second cycle of loading to drift ratios of 1, 1.5, 2, and 3%. For T1, E_h^+ (stem in compression) values of 0.11, 0.19, 0.20, and 0.22 were associated with drift ratios of 1, 1.5, 2, and 3%, respectively. Values of E_h^- (stem in tension) were approximately 10% lower than E_h^+. For walls with high-strength reinforcement (T2 through T6) and drift ratios between 1 and 2%, the average values of E_h were approximately 70% of the value of E_h for the wall with conventional reinforcement (T1).

CONCLUSIONS

Six large-scale reinforced concrete T-shaped slender walls were tested under reversed cyclic loading. The walls were proportioned and detailed to exhibit a ductile response. Axial loads were limited to the weight of the loading apparatus and self-weight. Based on the test data, the following conclusions are reached:

1. Walls designed for similar flexural strengths using Grade 60, 100, or 120 (420, 690, or 830) primary longitudinal reinforcement with similar tensile-to-yield strength ratio (f_t/f_y), uniform elongation (ε_{su}) not less than 6%, and fracture elongation (ε_{sf}) not less than 10%, exhibited similar strength and deformation capacity. This is evidenced by T1 (f_t/f_y = 1.34) and T4 (f_t/f_y = 1.36), which had drift ratio capacities of 3.7 and 3.9% and T3 (f_t/f_y = 1.23) and T6 (f_t/f_y = 1.18), which had drift ratio capacities of 3.0 and 3.1%, respectively.

2. Walls under low axial and shear stresses using reinforcement with $f_t/f_y \geq 1.18$, $\varepsilon_{su} \geq 6\%$, and $\varepsilon_{sf} \geq 10\%$ had drift ratio capacities of at least 3%. Among specimens satisfying these requirements, drift ratio capacity was not strongly correlated with either uniform or fracture elongation because the drift ratio capacity of these walls was limited by fracture of bars that had already buckled. The deformation capacity of specimens using reinforcement with $\varepsilon_{su} < 6\%$ or $\varepsilon_{sf} < 10\%$ was limited by sudden fracture of bars that had not previously buckled.

3. The initial stiffness K_e of walls designed for similar flexural strength using high-strength reinforcement Grade 100 (690) or 120 (830) was approximately 70% of K_e for T1 with Grade 60 (420) steel bars. In addition, during loading cycles to drift ratios of 1, 1.5, and 2%, the hysteretic energy dissipation index (E_h) for walls with high-strength reinforcement was on average 70% of E_h for T1. Additional studies are needed to investigate the combined effects of reduced K_e and E_h on the nonlinear dynamic response of wall systems with high-strength reinforcement.

AUTHOR BIOS

ACI member **Mohammad Sajedul Huq** *is Project Consultant at Simpson Gumpertz & Heger Inc., New York, NY. He received his BS in 2008 from Bangladesh University of Engineering and Technology, Dhaka, Bangladesh, and his PhD in 2018 from The University of Kansas, Lawrence, KS.*

ACI member **Erick A. Burgos** *is Senior Structural Designer at Rutherford + Chekene, San Francisco, CA. He received his BS in 2002 from Universidad Centroamericana José Simeón Cañas, El Salvador; his MS in 2006 from The State University of New York at Buffalo, Buffalo, NY; and his PhD in 2018 from the University of Kansas.*

ACI member **Rémy D. Lequesne** *is Associate Professor of Civil, Environmental & Architectural Engineering at The University of Kansas. He is Chair of ACI Committee 408, Bond and Development of Steel Reinforcement, and member of ACI Subcommittee 318-J, Structural Concrete Building Code—Joints and Connections, and Joint ACI-ASCE Committee 352, Joints and Connections in Monolithic Concrete Structures.*

Andrés Lepage, *FACI, is Professor of Civil, Environmental & Architectural Engineering at The University of Kansas. He is a member of ACI Committees 318, Structural Concrete Building Code; 374, Performance-Based Seismic Design of Concrete Buildings; 375, Performance-Based Design of Concrete Buildings for Wind Loads; and Joint ACI-ASCE Committee 335, Composite and Hybrid Structures.*

ACKNOWLEDGMENTS

Primary financial support was provided by the Charles Pankow Foundation and the Concrete Research Council of the ACI Foundation, under grant RGA #06-14. Additional support was provided by Commercial Metals Company, Concrete Reinforcing Steel Institute, Harris Rebar, Midwest Concrete Materials, Nucor Corporation, and The University of Kansas through the Department of Civil, Environmental & Architectural Engineering and the School of Engineering.

NOTATION

DR = drift (lateral displacement) divided by h_y
d_b = bar diameter, in. (mm)
E_c = modulus of elasticity of concrete, ksi (MPa)
E_h = hysteretic energy dissipation index, Eq. (2)
E_s = modulus of elasticity of reinforcement, ksi (MPa)
F_y = force associated with yield point, kip (kN)
f_c' = specified compressive strength of concrete, ksi (MPa)
f_{cm} = measured average compressive strength of concrete, ksi (MPa)
f_{ct} = measured average splitting tensile strength of concrete, ksi (MPa)
f_t = maximum tensile stress (tensile strength) of reinforcement, ksi (MPa)
f_y = yield stress of reinforcement, ksi (MPa)
G_c = shear modulus of concrete, taken as E_c/2.4, ksi (MPa)
h_w = height from base of wall (top of base block) to point of load application, in. (mm)
h_y = height from base of wall (top of base block) to top horizontal potentiometers, in. (mm)
I_{cr} = moment of inertia of cracked transformed section, in.^{4} (mm^4)
K_e = secant stiffness at $V = 0.8V_{max}$, kip/in. (kN/mm)
K_f = stiffness associated with flexural deformation, kip/in. (kN/mm)
K_{sp} = stiffness associated with strain penetration (into base block), kip/in. (kN/mm)
K_u = unloading stiffness, kip/in. (kN/mm)
K_v = stiffness associated with shear deformation, kip/in. (kN/mm)
ℓ_d = embedment length required to develop yield stress of reinforcement, in. (mm)
ℓ_w = length of wall section in direction of shear force, in. (mm)
M_n = nominal flexural strength calculated for a maximum concrete compressive strain of 0.003 and perfectly elastoplastic reinforcement, ft-kip (m-kN)
t_w = thickness of wall stem, in. (mm)
V_e = shear associated with M_n for measured material properties and shear span h_w, kip (kN)
V_m = shear associated with Δ_m, kip (kN)
V_{max} = maximum measured shear force per loading direction, kip (kN)
V_n = nominal shear strength, kip (kN)
W = hysteretic energy dissipated during half cycle of loading, in.-kip (mm-kN)
$X_{cg,cr}$ = distance from extreme compression fiber to neutral axis depth of cracked section transformed to concrete, in. (mm)
Δ_m = peak displacement during half cycle of loading, in. (mm)
δ_{base} = horizontal displacement of base block, in. (mm)
δ_{top} = horizontal displacement measured by top horizontal potentiometers, in. (mm)
ε_{sf} = fracture elongation of reinforcement
ε_{su} = uniform elongation of reinforcement or strain corresponding to f_t
ϕ_K = ratio of effective shear stiffness to uncracked shear stiffness; refer to 7.14 (Shear Stiffness) in Moehle[20]
λ = number of bar diameters over which yield strain of reinforcement is assumed to occur uniformly
θ_{base} = rotation of base block about an axis normal to plane of the wall stem, rad
ρ_ℓ = ratio of area of distributed longitudinal reinforcement to gross concrete area
ρ_t = ratio of area of distributed transverse reinforcement to gross concrete area

REFERENCES

1. ACI Committee 318, "Building Code Requirements for Structural Concrete (ACI 318-14) and Commentary (ACI 318R-14)," American Concrete Institute, Farmington Hills, MI, 2014, 520 pp.

2. Tavallali, H.; Lepage, A.; Rautenberg, J. M.; and Pujol, S., "Concrete Beams Reinforced with High-Strength Steel Subjected to Displacement Reversals," *ACI Structural Journal*, V. 111, No. 5, Sept.-Oct. 2014, pp. 1037-1047. doi: 10.14359/51686967

3. Moehle, J. P., and To, D. V., "Performance Characterization of Beams with High-Strength Reinforcement," RGA #04-14, Charles Pankow Foundation, Vancouver, WA, 2017.

4. Rautenberg, J. M.; Pujol, S.; Tavallali, H.; and Lepage, A., "Drift Capacity of Concrete Columns Reinforced with High-Strength Steel," *ACI Structural Journal*, V. 110, No. 2, Mar.-Apr. 2013, pp. 307-317. doi: 10.14359/51684410

5. Sokoli, D., and Ghannoum, W. M., "High-Strength Reinforcement in Columns under High Shear Stresses," *ACI Structural Journal*, V. 113, No. 3, May-June 2016, pp. 605-614. doi: 10.14359/51688203

6. FEMA 461, "Interim Testing Protocols for Determining the Seismic Performance Characteristics of Structural and Nonstructural Components," Federal Emergency Management Agency, Washington, DC, 2007.

7. ASTM A370-17, "Standard Test Methods and Definitions for Mechanical Testing of Steel Products," ASTM International, West Conshohocken, PA, 2017.

8. ASTM E8/E8M-16, "Standard Test Methods for Tension Testing of Metallic Materials," ASTM International, West Conshohocken, PA, 2016.

9. Huq, M. S.; Weber-Kamin, A.; Ameen, S.; Lequesne, R.; and Lepage, A., "High-Strength Steel Bars in Earthquake-Resistant T-Shaped Concrete Walls," SM Report No. 128, The University of Kansas Center for Research, Inc., Lawrence, KS, 2018.

10. Burgos, E. A.; Lequesne, R. D.; and Lepage, A., "Earthquake-Resistant T-Shaped Concrete Walls with High-Strength Steel Bars," SM Report No. 142, The University of Kansas Center for Research, Inc., Lawrence, KS, 2020.

11. ATC 115, "Roadmap for the Use of High-Strength Reinforcement in Reinforced Concrete Design," Applied Technology Council, Redwood City, CA, 2014.

12. ACI Committee 408, "Bond and Development of Straight Reinforcing Bars in Tension (ACI 408R-03)," American Concrete Institute, Farmington Hills, MI, 2003, 49 pp.

13. ASTM A706/A706M-16, "Standard Specification for Deformed and Plain Low-Alloy Steel Bars for Concrete Reinforcement," ASTM International, West Conshohocken, PA, 2016.

14. ASTM A615/A615M-16, "Standard Specification for Deformed and Plain Carbon-Steel Bars for Concrete Reinforcement," ASTM International, West Conshohocken, PA, 2016.

15. ASTM A1035/A1035M-16, "Standard Specification for Deformed and Plain, Low-Carbon, Chromium, Steel Bars for Concrete Reinforcement," ASTM International, West Conshohocken, PA, 2016.

16. ASTM C39/C39M-17, "Standard Test Method for Compressive Strength of Cylindrical Concrete Specimens," ASTM International, West Conshohocken, PA, 2017.

17. ASTM C496/C496M-11, "Standard Test Method for Splitting Tensile Strength of Cylindrical Concrete Specimens," ASTM International, West Conshohocken, PA, 2011.

18. ASCE/SEI 41-17, "Seismic Evaluation and Retrofit of Existing Buildings," American Society of Civil Engineers, Reston, VA, 2017.

19. Otani, S., "Hysteresis Models of Reinforced Concrete for Earthquake Response Analysis," *Journal of the Faculty of Engineering, The University of Tokyo*, V. 36, No. 2, 1981, pp. 125-159.

20. Moehle, J., *Seismic Design of Reinforced Concrete Buildings*, McGraw-Hill Education, 2015.

21. Fenwick, R., and Bull, D., "What is the Stiffness of Reinforced Concrete Walls?" *SESOC Journal*, V. 13, No. 2, 2000, pp. 23-32.

22. Sozen, M. A., and Moehle, J. P., "Stiffness of Reinforced Concrete Walls Resisting In-Plane Shear (EPRI TR-102731)," Tier 1 Electric Power Research Institute, Palo Alto, CA, 1993.

23. ATC 72, "Modeling and Acceptance Criteria for Seismic Design and Analysis of Tall Buildings," Applied Technology Council, Redwood City, CA, 2010.